Measuring Redshifts of Emission-line Galaxies

Using Ramp Filters

Ryan William Lesser

A senior thesis submitted to the faculty of
Brigham Young University
in partial fulfillment of the requirements for the degree of

Bachelor of Science

Joseph Moody, Advisor

Department of Physics and Astronomy

Brigham Young University

April 2016

ABSTRACT

Measuring Redshifts of Emission-line Galaxies
Using Ramp Filters

Ryan William Lesser
Department of Physics and Astronomy, BYU
Bachelor of Science

Photometric redshifts are routinely obtained for galaxies without spectral emission lines using broadband photometry. However, this method does not work if galaxies have emission. For galaxies with emission, it is theoretically possible to obtain reasonably accurate (< 500 km·s^{-1}) photometric redshift values using "ramp" filters. Such filters have a linearly increasing/decreasing transmission through the bandpass, causing the intensity of the image to be a function of the wavelength of the emission line. We have obtained a set of ramp filters tuned for isolating H-alpha at a redshift range of 3,000–9,000 km·s^{-1}. The set consists of two filters that are nearly linear in transmission, have opposite slope, and cover the wavelength range from 655–680 nm. We add a 2.1 nm FWHM filter centered on the red side of the ramp filters at 697 nm to measure the continuum. Redshifts are derived from the ratio of the ramp filters indices after the continuum has been removed. We recover the redshifts of a test sample of 16 Sey I and Sey II galaxies with an accuracy of 450 km·s^{-1}. This value can be improved by increasing the wavelength coverage of the ramp filters and measuring the continuum on the blue side as well.

Keywords: galaxies: distances and redshifts, galaxies: emission lines, galaxies:photometry, methods: observational

ACKNOWLEDGMENTS

I would like to thank Dr. Joseph Moody for advising me throughout this project and his continual guidance in helping me to develop my ideas. As an instructor, he has taught me what it means to be an astronomer – how one learns from failures and how to push forward with diligence toward credible discovery. I acknowledge Brigham Young University and the department of Physics and Astronomy for funding this project and for providing the resources we used to arrive at our results. I also thank John Bohman as my research partner for working heavily on data analyzation and making the majority of figures, Dr. Michael Joner of the astronomy department for obtaining data from the West Mountian Observatory, and Dr. Matt Asplund of the chemsitry department for scanning the ramp filters to obtain their traces in transmission.

Contents

List of Figures

List of Tables

Chapter 1

Introduction

1.1 Motivation

Galaxy surveys address cosmological questions of deep space. These questions include: How fast is the universe expanding? What is dark matter and how does it relate to baryonic matter? How does galaxy and large-scale structure evolve over time? To answer these questions, it is important to know how all kinds of matter, both visible and invisible, are distributed throughout the universe. This knowledge is essential to understanding the physics governing currently unexplainable phenomena, such as dark energy. A fundamental component is distance, which we gain through measuring redshifts.

Redshift surveys have shown the universe to have a honeycomb structure with clusters and filaments of galaxies surrounding empty spaces. The size and nature of galaxy clusters has confirmed the existence of dark matter, particularly dark matter in a low kinetic or "cold" state. Also, the galaxy-redshift relation has confirmed the presence of an accelerating force, or dark energy, which is described by a non-zero cosmological constant called Λ. The standard theory of cosmology is called "ΛCDM" to represent cold dark matter and a cosmological constant.

The ΛCDM theories predict that galaxy structures form at places where dark matter is most dense. Not knowing exactly how dense the dark matter needs to be, a bias factor, b, is empirically assigned to relate dark matter density to galaxy formation. Densities above this value lead to galaxy formation, while densities below it do not. The best place to study the bias factor is in the lowest density volumes or galaxy "voids." Some galaxy formation theories predict that voids should be completely empty because dark matter did not become dense enough there (e.g. Tinker & Conroy 2009). Other theories predict there should be hundreds of dwarf galaxies within the voids (e.g. Tikhonov & Klypin 2009, Kreckel, Joung, and Cen 2011). The presence or absence of dwarf galaxies in voids then is a powerful diagnostic of galaxy formation and their implications for dark matter and ΛCDM models.

Galaxies in voids are expected to be small, low-mass dwarfs with recent star formation. A glaring weakness of current redshift surveys is the frequent omission of dwarf galaxies, since the apparent magnitudes of such objects are too faint to be included. For example, the SDSS spectroscopic survey measured galaxies to a magnitude of 17.77 which is sufficient to locate the theoretically interesting dwarf galaxies with absolute magnitude M_r fainter than –14 only out to a redshift of 1,700 km·s^{-1}. (SDSS Data Release 7 2013) The closest well-defined void centers are beyond a redshift of 4,000 km·s^{-1}. Therefore, we are missing important information these galaxies have to offer in our mission to answer the questions posed above.

The goal of future research is to better understand the distribution of dwarf galaxies throughout clusters and voids. Because dwarf galaxies are generally the type of galaxy to be found within voids, they become landmarks for mapping voids and measuring how they expand in relation to superclusters (Draper et al. 2016). However, the closest well-defined void centers are beyond a redshift of 4,000 km·s^{-1}. Dwarf galaxies have been found in the Lynx-Cancer void, but this is more of a low-density region than the large-scale voids we are interested in (Pustilnik & Tepliakova 2011). For these reasons, a method of deriving redshifts geared towards dwarf galaxies would be

of great value to the astronomical community.

1.2 Introduction to Methods

The only methods used for obtaining redshifts are photometry and spectroscopy. Each has its advantages and disadvantages, making them more favorable depending on the type of galaxy being observed. Over the years, several improvements have been made in both photometric and spectroscopic methods, and each has taken its turn in favorability by those conducting surveys.

Spectrometers work by using a grating or prism to split light from a single galaxy into a spectrum, making emission and absorption lines easily identifiable. By comparing shifted lines to their rest wavelength, one can calculate a redshift. This method offers a high degree of accuracy because spectral features can be finely discriminated when these comparisons are made. Multi-fiber spectrometers have made observing faster and efficient and over 1.4 million spectroscopic redshifts have been obtained. However, this is still a tiny fraction of the universe. Spectrometers work best in galaxy clusters where there are many targets within a single field of view. Spectroscopy is time-consuming and inefficient when many objects need to be observed, especially for voids where galaxies are sparse. Spectrometers themselves are extremely expensive and telescopes that best use them are large. Therefore, many people compete for time on their use. For our purposes of surveying dwarf galaxies (which are more numerous than standard galaxies), it would be impractical to apply for the time needed to survey them all. If voids are to be surveyed, we must use another method that can obtain redshifts in a more efficient manner.

The photometry method was first developed by Baum 1962 in which spectral energy distributions (SEDs) of galaxies were observed using a photometer. The SEDs are plotted on the same graph as SEDs for nearby galaxies in the Virgo cluster using a logarithmic scale for wavelength. The Virgo galaxies are relatively stationary with respect to the Milky Way, making them useful as

a reference for comparison. Redshifts are then derived from the displacement between the SEDs of the Virgo galaxies and the galaxies in question. Other photometric methods include color-color diagrams (Koo 1985 and Pello et al. 1996), template fitting (Loh and Spillar 1986), linear regression (Connolly et al. 1995), and more recently, prediction tree algorithms (Kind and Brunner 2013) and artificial neural networks (Collister and Lahav 2008). Advantages to photometry are high signal-to-noise ratios and that information on potentially thousands of objects can be gathered in one field of view. In general, photometry can work on objects up to five magnitudes fainter than spectroscopy taken with the same telescope. One disadvantage of photometric methods is that wavelength resolution is inversely proportional to the width of the filter's bandpass. This factor limits the accuracy of our method to 500 $\text{km}\cdot\text{s}^{-1}$ or worse. A second disadvantage is that photometry does not work on galaxies with strong emission lines, and dwarf galaxies have strong emission lines.

We have designed a photometric method capable of handling galaxies with emission lines where line strength is directly proportional to the accuracy of the redshifts we obtain. It will work for galaxies that are inherently faint, if the lines are strong enough to be detected and will allow us to calculate redshifts for any galaxy of strong Hα emission with line EW > 25. No such method has ever been conducted at Brigham Young University nor published abroad in the literature. Because this is the first time it is used, it must be calibrated and proven accurate. Therefore, our research aims to evaluate our method's viability first by testing it on several luminous galaxies of strong emission and well-known redshift. By comparing the redshift values we obtain from our method with the published values, we can ascertain its accuracy.

In chapter 2, we will discuss how the method works. In chapter 3, we share our results from the galaxies on which it was tested as well as describe its susceptibilities and the errors we obtain. Finally in chapter 4, we discuss ways we can improve upon the method to obtain higher accuracy and broaden its range of sensitivity.

Chapter 2

Methods

2.1 Ramp Filter Method

If faint dwarf galaxies are to be observed and accurate redshifts derived, it will be important to select a strong emission line that can stand out amidst the ubiquitous continuum observed in all galaxies. The Hα line, centered at 656.2 nm, is the most prominent line in galaxies with emission and is widely used across surveys to derive redshift. Therefore, we chose to isolate this line and based our method around it.

Our method utilizes three filters. The first two filters span 640–685 nm and slope in transmission approximately linearly but with opposite slope. Their crossover point is located at 665nm (See Figure 2.1). The filter imaging more in longer wavelengths we call the red-sloping (RS) filter because it slopes up to the red. The filter imaging shorter wavelengths we call the blue-sloping (BS) filter and it slopes up to the blue. The filters' slope is slightly concave up and becomes curvilinear near both ends of the bandpass.

Because the solution is a function of line strength, it is essential to subtract out the continuum from the ramp filters. Doing so puts all emission lines on a flat frame of reference so that only

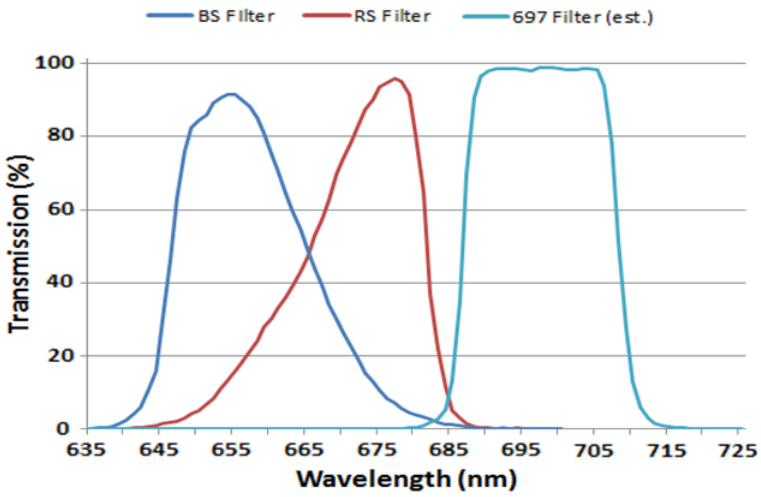

Figure 2.1 Transmission of light through each filter according to wavelength. The blue curve is of the blue-sloping (BS) filter, the red curve is of the red-sloping (RS) filter, and the turquoise curve is of the continuum (697) filter. The continuum filter is depicted with a theoretical trace based on a similar filter.

line strength contributes to the measured intensity from each filter. To estimate the continuum we use a 2.1 nm FWHM filter designed for Active Galactic Nuclei (AGN) reverberation mapping centered at 697 nm. Because the wavelengths within the ramp filter bandpass contain an emission line, we had to measure the continuum outside this region. At these wavelengths the continuum is approximately a flat line. Hence, the 697 filter — being so close to the red side of the ramp filters —provided an ideal estimate of the continuum value inside the ramp filters' bandpass.

Redshifts are obtained from the ratio of the continuum-corrected BS and RS filters. Because solutions can only be obtained for lines within the wavelength range of the filters, there is a limitation to the range of redshifts that can be derived accurately. Our method is capable of measuring redshifts between 3,000 and 9,000 km·s^{-1}. This is a suitable range, given that the centers of candidate voids for future study containing dwarf galaxies are located between 4,550 and 4,980 km·s^{-1} with diameters of approximately 4,000 km·s^{-1}.

2.2 Observations

Seyferts' strong Hα lines make them a natural choice for observation. Using the BYU 0.9 m telescope at West Mountain Observatory, we obtained data for 16 Seyfert I and II galaxies of known redshifts between 3,500 and 9,000 km·s^{-1}. Images were obtained between June 13–27 of 2015. The initial list of candidates for observation was longer than 100, with the majority being Seyfert galaxies. Unfortunately, our method requires perfect photometric conditions to produce any accurate results. This is because no standard stars have yet been calibrated with this method, therefore it is necessary to rely on perfect photometric conditions so that our frame of reference for each object is the same from night to night. Though data was collected on more than 60 of these galaxies, most of them had to be thrown out because even light clouds destroyed photometric accuracy. Once this method is calibrated, it will work for less than perfect conditions.

Of the 16 Seyferts observed on perfect photometric nights, all had $m_v < 15.0$ and Hα line strengths with FWHMs greater than 25 Å. We exposed for 2–3 minutes in both the RS and BS filters and 10 minutes in the 697 filter. It was necessary to expose longer in the continuum, as the solution is highly sensitive to and dependent on the accuracy to which we measure it, as will be explained in chapter 3. Data were reduced using standard IRAF procedures and photometry was performed using MIRA. The inner photometric aperatures for each galaxy were placed close enoguh to maximize signal with radii between 2.5–3″, with the sky subtraction annulus situated well outside the galaxy.

Chapter 3

Results

3.1 Relationship between Ratio and Redshift

In this section, we examine the correlation between the ratio of the intensities of the two ramp filters and the redshift they yield. We study the effect of these ratios on the solution near the linear portions of filter transmission as well as close to the curved ends. In section 3.2 we report the errors in our method both qualitatively and quantitatively, and discuss the sources that contribute to that error.

A strong relationship between the continuum-corrected BS/RS ratio and the redshift is crucial to our method's viability. We show this relationship by taking the data listed in Table 3.1 and plotting the ratio vs. published redshift for each galaxy (See Figure 3.1). The data points are fit with a third-order polynomial, which best shows the correlation. We observe that galaxies in the linear portions of the graph with redshifts between 3,000 and 9,000 km·s^{-1} are the galaxies whose emission lines fall within the physical linear portions of the sloped filters' transmission curve (See Figure 2.1). The standard deviation of the data within these ranges was calculated to be 450 km·s^{-1}. This value is acceptable for the purposes of redshift surveys and establishes a

Table 3.1 The 16 Seyfert galaxies imaged through our filter set with associated apparent magnitudes in the B-band, published redshifts, derived redshifts, and error between the published and derived values.

Galaxy	Type	B	Published cz (km·s^{-1})	Derived cz (km·s^{-1})	Error (Δcz)
Mrk 686	Sey 2	14.55	4242	4121	-121
NGC 5548	Sey 1	14.35	4877	4739	-138
Mrk 266SW	LINER	14.19	8564	8297	-267
NGC 6786	Sey 2	13.7	7500	7949	449
NGC 2650	Sey 2	14.3	3839	4054	215
NGC 5765	Sey 2	14.6	8345	7968	-376
NGC 5990	Sey 2	13.1	3765	4047	282
NGC 6521	Sey 2	14.3	8202	7251	-951
Z 229-015	Sey 1	15.4	8253	8212	-41
Z 493-002	Sey 2	15.6	7529	8100	572
Mrk 461	Sey 2	14.5	4977	4415	-562
NGC 5674	Sey 2	13.7	7493	7395	-98
IC 1368	Sey 2	14.3	3912	4666	754
II ZW 102	Sey 2	15.39	7885	7680	-205
NGC 3822	Sey 2	13.7	6122	5788	-333
NGC 5515	Sey 2	13.7	7743	6931	-812

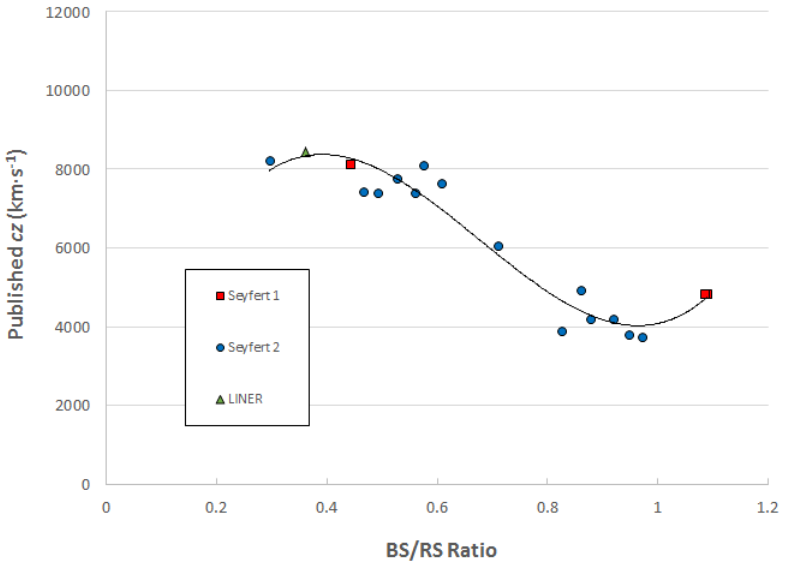

Figure 3.1 The relation between the continuum-corrected BS/RS ratio and redshift. Each dot represents a galaxy observed using the ramp filters, where type of galaxy is distinguished in the legend by shape and color. A third-order polynomial curve was fit to the data with a standard deviation of 450 km·s^{-1}.

correlation between ramp filter ratio and redshift, demonstrating that the goal of the research has been achieved — to derive an accurate redshift. Likewise, the curvilinear portions of Figure 3.1 correlate to the wavelength ranges for which lines are getting close to the curvilinear portions of the sloped filters' transmission curve where the solution degrades. Therefore, we rejected lines redshifted below 3,500 or above 9,000 km·s^{-1}. The reason there are more data points on the outer edges and only one near the center is because there are simply fewer galaxies found at those mid-ranges compared to the clusters located at the extremes.

To see how well our derived redshifts match with the published values, we then made a plot using these two values for the axes in Figure 3.2. Note that a perfect one-to-one correspondence would be a line with a slope of one, modeled with the dotted line. Our solution comes very close to the ideal with a slope of 0.92 and is shown by the solid line. Two galaxies were imaged twice, and

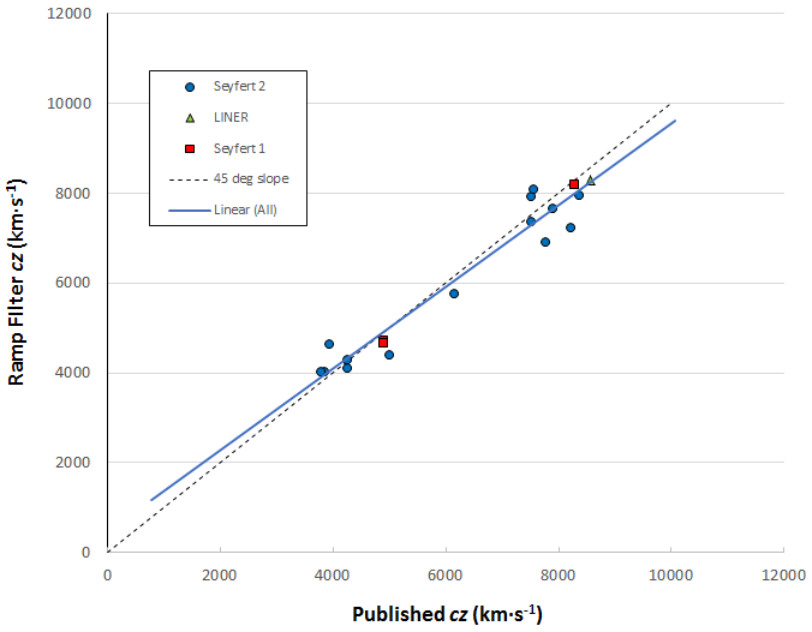

Figure 3.2 The derived redshift values vs published values for 16 Sey I and Sey II galaxies. Type of galaxy is distinguished in the legend by shape and color. The dotted line is situated at 45 degrees, modeling an ideal fit between derived and published redshifts. The blue line is our actual fit for all data points.

the difference between the redshifts obtained the second time were no greater than 100 km·s^{-1}. This shows that our method is precise and repeatable. Again, the standard deviation of the data is 450 km·s^{-1}.

3.2 Errors

Because of the many variables involved in our method, it is important to determine how each one affects the error in our solution. Among these variables are the error measured in the continuum, line strength, and position of the line within the bandpass. In section 3.1, we mentioned the effect of the emission line being within a linear portion of the ramp filter's transmission as opposed to a

curved portion near the end. This error is always present near the limits of any filter set.

Of concern is the accuracy to which we measure the continuum. An error in measuring the continuum translates to an error in redshift that is a function of line placement within the filter, or redshift itself. The error in redshift is also a function of line strength. To examine the effect of line placement quantitatively, we plot the wavelength of the emission line versus cz while holding error in the continuum at a constant value of 1%.(Figure 3.3)

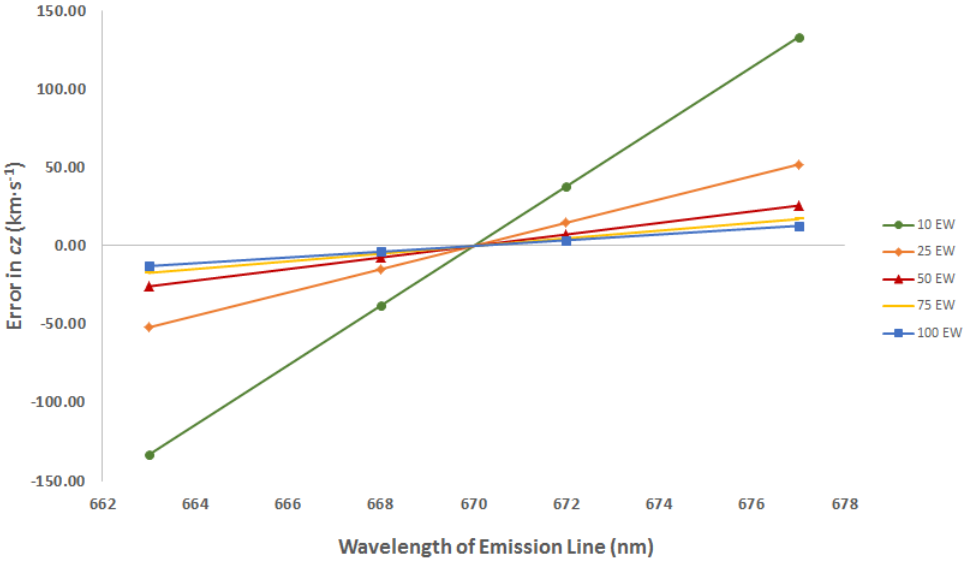

Figure 3.3 The expected error in redshift as a function of the emission line's central wavelength within the bandpass. This is specifically for an error in the measured continuum of 1%. Different colors show the relationship for various line strengths.

Lines of different equivalent width are plotted with different colors to show how error changes with line strength. As can be seen, the error is essentially zero for all line strengths at 670 nm, which is the crossover point of the BS and RS filter (the place where both filters have a transmission $\approx 50\%$). Zero error at this point is a result of both ramp filters measuring the same amount of continuum — thus when the BS/RS ratio is taken, the continuum value simply divides out. This

means that for a line of any strength, the ramp filter method will have zero error for a line located exactly at the crossover point. Going in either direction out from this wavelength, the error increases linearly to the filter limits, which for our filter set includes a range of 662–678 nm. Note that line strength plays an important role in the accuracy, with error remaining reasonably small for EW > 25, regardless of the cz value.

The previous graph was held at a constant error in continuum of 1%. To investigate the effect of increasing the error in the continuum, we graph the error in redshift versus the error in continuum, holding cz constant. We arbitrarily pick a cz value of 5357 since it corresponds to a line between the blue filter limit and the crossover point where typical data are expected to be. This graph is plotted in Figure 3.4, again using multiple colors to show lines of varying equivalent width.

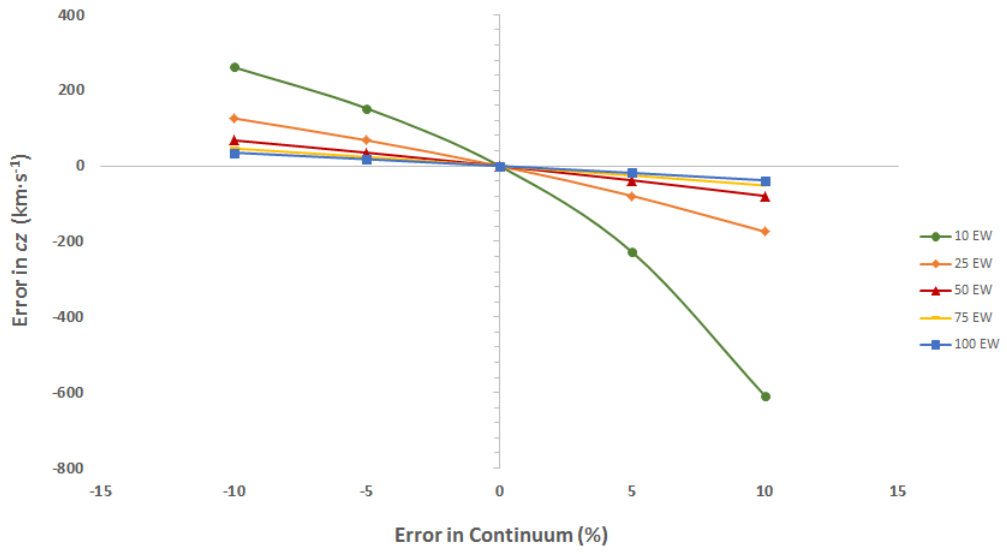

Figure 3.4 The expected error in redshift for a line at 668 nm (cz = 5357 km·s^{-1}) as a function of error in the continuum. Different colors show the relationship for various line strengths.

Like Figure 3.3, there is also a point at which error in redshift goes to zero. This is obviously when the error in the continuum is measured with zero error. For strong lines (> 25 EW), errors

are marginal for a continuum error < 10%. However, when we compare the effect of error in the continuum to placement of the line within the bandpass, the effect of error in the continuum is much stronger. In other words, changing error in the continuum by a few percent introduces more error than changing the line placement by a few nanometers. We also learn that to keep our expected errors manageable, we should not expect to measure galaxies with Hα emission lines smaller than about EW $= 25$ Å.

Chapter 4

Discussion and Conclusions

4.1 Conclusions

We conclude that accurate redshifts using the ramp filter method are obtainable over the wavelength range of the ramp filters' bandpass, which for our method corresponds to a redshift range of 3,000–9,000 km·s^{-1}. These redshifts match the published values to an accuracy of 450 km·s^{-1}. This is acceptable for exploring voids of diameters > 4,000 km·s^{-1}. The method proved to be very repeatable, with derived redshifts for repeat galaxies differing by less than 100 km·s^{-1}.

This method's weaknesses include a high sensitivity to the continuum measure, solution degeneracy near the slope ends, and dependency on perfect photometric conditions. Its strengths include saving time through its ability to obtain redshifts from multiple galaxies within a single field of view, reducing cost compared to other spectroscopic methods, and finding redshifts for galaxies with emission lines. The latter allows this method to be used on galaxies often excluded from photometric redshift surveys, such as dwarf galaxies.

4.2 Directions for Future Work

In the future, we believe obtaining a wider filter set would avoid solution degradation and degeneracy for lines near the slope ends. We plan to purchase such a filter set and use it to improve accuracies by refining the relation between the BS/RS ratio and redshift. This will require about two weeks of observations.

In this work, we have proven that galaxies with known emission and redshift can have their redshifts measured. The next step is to understand how all the objects detected on a single image of the sky register and appear in our filter set. It is possible that some stars having large absorption bands will register false positives. We need to sort out such objects probably by adding broadband photometry to the data using the ramp filters.

Much of the data had to be thrown out because perfect photometric conditions were not achieved. We will explore ways of calibrating our galaxies against the mean population in the field. This "differential photometry" should enable us to obtain reasonable data without requiring perfect conditions.

Having shown this method's crucial dependence on an accurate continuum measure, we also plan to better estimate the continuum in one of two ways. One is to place an additional continuum filter on the blue side of the ramp filters and compute an average value for the continuum between both continuum filters. Another is to obtain a double-notch continuum filter where an average would be obtained from a single image. Because the notches' bandpass cannot overlap with the ramp filters' bandpass, we will place the notches as close as possible to the red and blue side of the ramp filters to get the best possible estimate. This would save more time than the first option, however it would be necessary to make sure an average continuum value from a single filter yields an accurate measure.

The calibration of this method is ongoing. As soon as it is finished, we will begin testing its originally intended purpose by conducting surveys of dwarf galaxies in nearby voids.

Bibliography

Baum, W.A., in G.C. McVittie (ed.) 1962, Problems of extra-galactic research, p. 390, IAU Symposium No.15

Collister, A.A., & Lahav, O. 2008, in preparation

Connolly, A.J., Csabai, I., and Szalay, A.S. 1995, AJ, 110, 6

Draper, C., Moody, J. W., McNeil, S.M., and Joner, M. 2016, in preparation

Kind, M.C. & Brunner, R.J. 2013, MNRAS, 000, 1–21

Koo, D.C. 1985, AJ, 90, 3

Loh, E.D. & Spillar, E.J. 1986, ApJ, 303, 154–161

Pello, R., Miralles, J.M., Le Borgne, J.F., Picat, J.P., Soucail, G., and Bruzual, G. 1996, A&A, 314, 73–86

Pustilnik, S. A. & Tepliakova, A. L. 2011, MNRAS, 415, 1188

SDSS Data Release 7, Sloan Digitial Sky Survey, http://classic.sdss.org/dr7/

Tikhonov, A.V. & Klypin, A. 2009, MNRAS, 395, 1915

Tinker, J.L., & Conroy, C. 2009, ApJ, 691, 633

Index